Energy 297 (2024) 131183

Contents lists available at ScienceDirect

Energy

journal homepage: www.elsevier.com/locate/energy

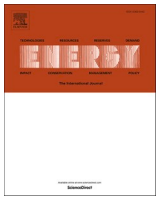

Effect of heating rate on the secondary reaction in low-rank coals pyrolysis with the real-time evolution analysis of in-situ tar

Yao Zhu, Qinhui Wang *, Jiqing Yan, Jianmeng Cen, Mengxiang Fang

State Key Laboratory of Clean Energy Utilization, Zhejiang University, Hangzhou, 310027, China

ARTICLE INFO

Handling Editor: Wojciech Stanek

Keywords:
Heating rate
Online evolution law of volatiles
Low-rank coal
Pyrolysis mechanism
Secondary reaction

ABSTRACT

Performing online evolution analysis of tar in actual pyrolysis process is a major challenge. In this work, the effects of heating rate (HR) on evolution curves of in-situ tar for low-rank coals pyrolysis were investigated in a novel laboratory bench. The escape law of volatiles was obtained, the influence of HR on secondary reactions was analyzed, the association between products and molecular structures was constructed, and pyrolysis mechanism was deduced. Aliphatic hydrocarbons (except dienes), phenols, and oxygenated compounds have only one peak, while dienes and aromatics have multiple peaks throughout the pyrolysis process. The first peak is attributed to coal primary pyrolysis. At increased HRs, the second peak for 1~2ring aromatics is from the cracking of primary volatiles, and that for 3~4ring aromatics from coal continued cracking. The proportion of phenols and oxygenated compounds decreases, aromatics increases, and aliphatic hydrocarbons varies for different coals. Generally, HR increases the yield of primary volatiles by enhancing coal primary pyrolysis, elevates the proportion of light aromatics by promoting secondary cracking and aromatization of primary volatiles, reduces char yield by inhibiting condensation reactions throughout the pyrolysis process. The similar macromolecular structures of different coals make the evolution curve versus HRs follow a common law.

1. Introduction

The shortage of oil resources and high proportion and low utilization rate of coal are the general utilization landscape of China's energy [1]. The low-rank coal accounts for more than 55% of coal resources in China [2]. Pyrolysis is one of the effective ways to alleviate the shortage of crude oil resources and improve energy utilization efficiency [3]. High value-added chemicals, especially aromatic compounds, can be separated from coal tar, so it is important to obtain high quality tar during the coal pyrolysis process [4,5].

Traditional tar detection methods such as gas chromatography/mass spectrometry (GC/MS) involve time-consuming chromatographic separation steps [4,6,7]. It is well known that coal tar is poorly stabilized due to the presence of a large number of reactive free radicals in the tar [8]. These steps contribute to variations in the original composition of tar product. Therefore, the method of analyzing pyrolysis characteristics and mechanism based on offline pyrolysis product composition and distribution needs to be improved. The pyrolysis-gas chromatography/mass spectrometry (PY-GC/MS) avoids the complex process of traditional tar detection but cannot realize online detection of tar during the thermochemical conversion process [9]. The online tar detection not only to obtain the product distribution of fresh in-situ tar, but also to obtain the release pattern and generation mechanism of volatiles during pyrolysis process, to construct the correlation between products and the molecular structure, and then to deduce the pyrolysis mechanism. Studies employed TG-MS to investigate online evolution patterns of gas molecules, but the commonly employed electron ionization (EI) generates large amounts of fragments and is not suitable for the online detection of tar macromolecule [10].

The development of vacuum ultraviolet photoionization technology to address the limitations of EI. The near-threshold photoionization reduces fragmentation on the mass spectra and guarantees the attribution of molecular ions peaks [10,11]. Table 1 summarizes relevant literatures in recent years. Some scholars have carried out relevant studies to provide solutions for the online detection of the tar and obtained innovative conclusions. However, there are still some limitations. Jia et al. used pyrolysis synchrotron vacuum ultraviolet photoionization mass spectrometry (Py-SVUV-PIMS) to analyze volatile products of bituminous coal pyrolysis [12]. However, they did not investigate the entire thermochemical conversion process thoroughly and performed

* Corresponding author.
E-mail address: qhwang@zju.edu.cn (Q. Wang).

https://doi.org/10.1016/j.energy.2024.131183
Received 23 September 2023; Received in revised form 22 February 2024; Accepted 1 April 2024
Available online 9 April 2024

Table 1
Summary of literatures on online detection of volatiles.

Sample	Equipment	Conditions	Research content	Ref.
Polyvinyl chloride	*Py-VUV-PIMS*	10 C/min, 10^{-5}pa	Release curve of primary pyrolysis products	[13]
Lignite	*Py-VUV-PIMS*	10 C/min, 10^{-5}pa	Release curve of primary pyrolysis products	[14]
Coal-model compounds	Py-VUV-PIMS	10 C/min, 10^{-5}pa	Primary pyrolysis product distribution and composition	[3]
Low rank coal	Py-VUV-PIMS	10 C/min, 10^{-5}pa	Evolution characteristics of primary pyrolysis products	[15]
Bituminous	Py−SVUV-PIMS	500~800 C, 10^{-1} pa	Pyrolysis products	[16]
Copolymer	Py−SVUV-PIMS	10 C/min, 10^{-1} pa	Temperature-evolved profiles of major products	[10]
Rice husk	Py−SVUV-PIMS	550 C, 10^{-1} pa	The time-evolution of typical compounds	[17]
Coal and corn	Py−SVUV-PIMS	10^{-1} pa	The pyrolysis processes of coal, corn, and coal-corn	[18]
Furfural	Py−SVUV-PIMS	10^{-1} pa	Theoretical calculations	[19]
Lignin	Py-TOF-MS	10^{-5} pa	In-situ detection on primary volatiles and stable radicals	[20]
Baiyinhua coal	Py-VUVPI-TOF-MS	10^{-4} pa	Coal pyrolysis products	[21]
Cigarette smoke	SPI-TOFMS	10^{-5} pa	Real-time measurements of VOCs	[22]

under isothermal conditions, making it difficult to observe the escape law of tar during the heating process. Zhang et al. analyzed the pyrolysis process of small molecular compounds and speculated on pyrolysis mechanism based on theoretical calculations [11]. Ban et al. selected several representative coal-related model compounds to determine the distribution and composition of primary pyrolysis products in the presence of catalysts by the in-situ pyrolysis vacuum ultraviolet photoionization time-of-flight mass spectrometry (Py-VUV-PIMS) [3]. However, the simple structure of samples limits the applicability of the results to the comprehensive analysis of coal pyrolysis processes. Moreover, it is worth noting that above studies are performed under negative pressure conditions, which greatly inhibits the occurrence of secondary reactions of volatiles. And the HR cannot be changed because of the limited equipment structure. Although the distribution and escape behavior of the primary product can be studied, it cannot reflect the evolution law of tar in the actual pyrolysis process, especially the lack of online detection of pyrolysis process at different heating rates (HRs). Analyzing the actual thermochemical conversion process by tar online detection is a major challenge.

Studies have shown that secondary reaction affects the tar yield and product distribution [23,24]. The HR is an important factor affecting the secondary reaction. There have been a large number of studies on the effect of HR on tar yield and composition, all based on offline tar detection methods [24–31]. Lievens et al. investigated the effect of HR (5–100 °C/min) on the tar distribution of lignite pyrolysis by PY-GC/MS and found that phenolic yield was approximately independent of HR at slow HR and low temperature [26]. While Li et al. conducted experiments using a downer-bed reactor and found that as the HR increased from 10 to 1000 °C/min, the phenols increased first and then decreased [29]. Although previous studies adopted many experimental and theoretical methods to explain the effects of HR on tar yield, the conclusions were still full of contradictions. The reason for the contradiction is that there are three secondary reaction regions, intra-granular, inter-granular and extra-granular, but offline tar detection method is unable to separate the three secondary reaction regions. However, the online tar detection method can reflect the effect of HR on the secondary reaction in different regions. Hence, it is necessary to study the online evolution law of tar macromolecules with the change of HR to understand correctly the coal pyrolysis process and provide more support for the basic principles of coal pyrolysis. Intra-granular secondary reactions are inevitable, while extra-granular secondary reactions can be controlled by modifying experimental conditions. Therefore, it is particularly important to suppress the extra-granular secondary reactions to study the intra-granular secondary reactions.

In summary, the effects of HR on tar were based on offline testing method, while the offline tar detection method could not reflect the effect of HR on the secondary reaction in different regions. At present, the relevant studies are performed under negative pressure conditions, which greatly inhibits the secondary reactions of volatiles. And the HR cannot be changed because of the limited equipment structure. It cannot reflect the tar evolution law in the actual pyrolysis process and lacks the release characteristics of volatiles with HR. To address the issues mentioned above, in this work, the effects of HR on the product distribution of in-situ tar and online evolution curves of volatiles for the pyrolysis of three low-rank coals were investigated. The pyrolysis experiments were conducted in a novel laboratory bench Thermogravimetric-Single Photon Ionization Time of Flight Mass Spectrometer/Electron Ionization Quadrupole Mass Spectrometer (TG-SPI-TOF-MS/EI-QMS). The escape pattern of volatiles was obtained from the real-time evolution curves, then the influence of HR on the internal secondary reaction was analyzed, the association between reaction products and molecular structures was constructed, and finally the pyrolysis mechanism was deduced.

2. Materials and methods

2.1. Materials

Three low-rank coals were ground and sieved to a particle size range of 75–125 μm. The properties of coals are shown in Table 2. It can be seen that Naomao Hu coal (NMH) has the highest volatile and O content, Runbei coal (RB) has the highest H content and Bosi Tan coal (BST) has the highest C content. They were dried at 105 °C for 24 h to remove the moisture before pyrolysis experiments.

2.2. Experimental equipment

The volatiles produced by low-rank coal pyrolysis were analyzed online using the SPI-TOF-MS and EI-QMS. Fig. 1 shows the schematic diagram of this system. A silica capillary with an inner diameter of 75

Table 2
Proximate and ultimate analyses of low-rank coals.

Sample	Proximate analysis (wt%)				Ultimate analysis (wt%, ad)				
	M	A	V	FC	C	H	O[a]	N	S
NMH	2.65	5.31	46.26	45.78	60.68	3.27	26.98	0.74	0.37
BST	1.98	5.02	38.94	54.06	76.55	3.65	11.00	1.43	0.37
RB	1.67	9.40	39.84	49.04	67.27	5.48	12.98	1.21	1.99

[a] by difference.

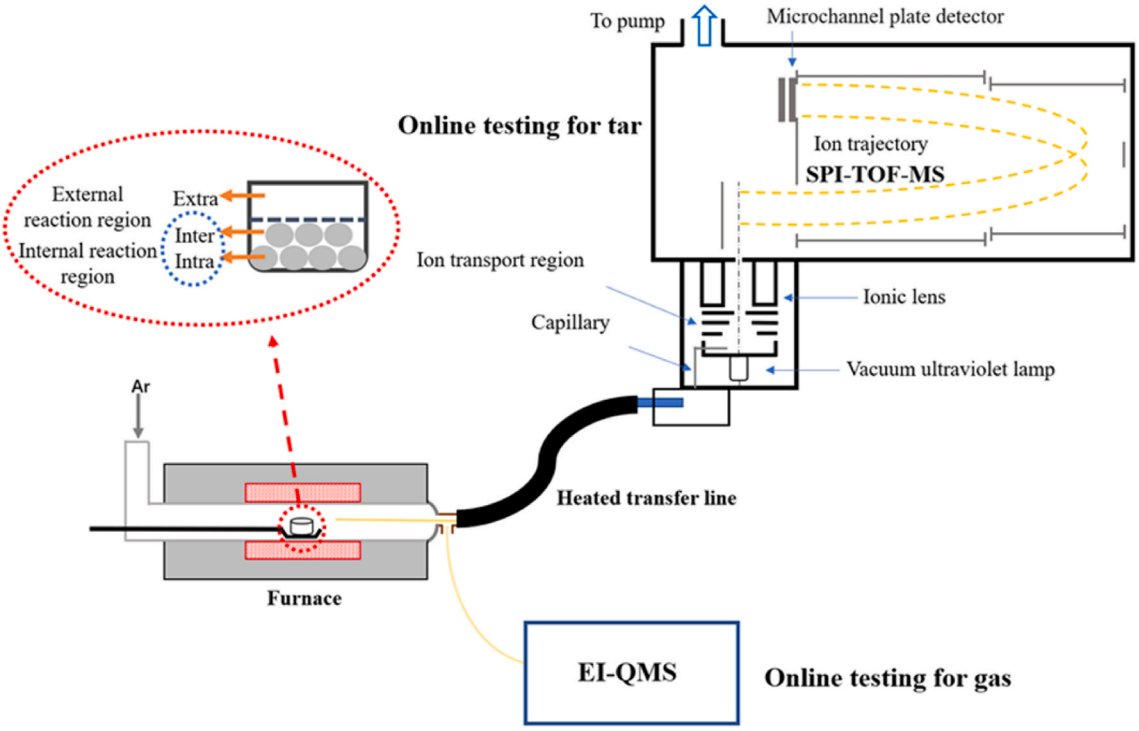

Fig. 1. Schematic diagram of the system.

μm is placed inside the transmission line to introduce the volatiles into the photoionization zone. The transmission line is heated to 220 °C to prevent condensation of the volatiles. The regions where the secondary reactions occur include intra-granular, inter-granular and extra-granular, as shown in Fig. 1. In order to investigate the impact of HR whilst avoiding secondary reactions outside the particles, the capillary tube in this experiment is positioned inside the reactor. The volatiles can enter the capillary tube immediately after escaping from the particles, and secondary reactions are negligible since the capillary tube is a vacuum environment. Additionally, the short transmission line allows volatiles to reach the detection zone quickly. Therefore, only intra-granular and inter-granular secondary reactions need to be considered, collectively referred to as the internal secondary reactions. The secondary reactions mentioned in the following text all refer to internal secondary reactions.

The volatiles are analyzed using a photon energy of 10.6 eV, which can ionize most organic compounds while minimizing fragmentation and yielding molecular ion peaks. The SPI-TOF-MS online analysis system can obtain two kinds of spectra: cumulative spectrum and time evolution spectrum. The cumulative spectrum reflects the species distribution of volatiles at a selected temperature, while the time evolution spectrum of volatiles reflects the evolution pattern of the signal intensity of a certain volatile matter throughout the pyrolysis process. The time evolution spectrum is recorded with 5s intervals. The EI-QMS is used for real-time monitoring of non-condensable gases.

2.3. Pyrolysis experiments

Pre-experiments showed that extremely slow HRs resulted in poor signal values and very large experimental errors, so HRs of 10, 30, 50 and 80 °C/min were used in this work. Based on the upper limit of the amount of sample that can be placed in the TG, the final experimental conditions are as follows. 20 mg of sample was placed in the crucible and purged with 50 mL/min of Ar for 30 min to replace the gas in the reactor completely. Then, the SPI-TOF-MS and EI-QMS baselines were observed for stability and after stabilization the experiment was continued at a flow rate of 50 mL/min. The final pyrolysis temperature was 800 °C and maintained for 20 min after reaching the final temperature to allow sufficient pyrolysis. SPI-TOF-MS and EI-QMS are used for real-time online detection of volatiles during pyrolysis process. The remaining char was collected after the experiment. Each set of experiments was repeated three times.

2.4. Analysis methods

The quantitative and qualitative analyses of the gases are as follows. The gases detected in this work include CO_2, CO, CH_4, and H_2. Accurate quantification is difficult due to the long pyrolysis time and the small amount of sample. In this work, a semi-quantitative method is used for gas quantification.

Due to the different intensities of ions signal, it is not possible to compare the contents of different compounds by comparing the ions intensity, but changes in the signal intensity of ions under different conditions can reflect the changes in the concentration of a certain compound [17]. The concentration of a particular compound is linearly related to its peak area for the same sample mass, so the variation in concentration of each component can be revealed by the change in the peak area. The relative peak area is calculated by dividing the peak area (target product) by the total peak area (all products detected). The change in the relative peak area of target product reveals the relative proportion of the target product among all detected products as reaction conditions change, allowing the effect of HR on this target product to be deduced.

The qualitative analysis is determined by combining the results of the PY-GC/MS analysis (shown in Supplementary material) with the physical and chemical properties of coal, as well as previous studies [12, 32–34]. The main products and their ionization energies (IEs) are listed in Table S1. In this work, tar components are divided into short-chain aliphatic hydrocarbons (C4–C10), long-chain aliphatic hydrocarbons (C11–C19), phenolic compounds (PHs), oxygenated compounds (OCs), and aromatic hydrocarbons, in which the aromatic hydrocarbons are divided into monocyclic (MAHs), bicyclic (BAHs) and polycyclic (PAHs,

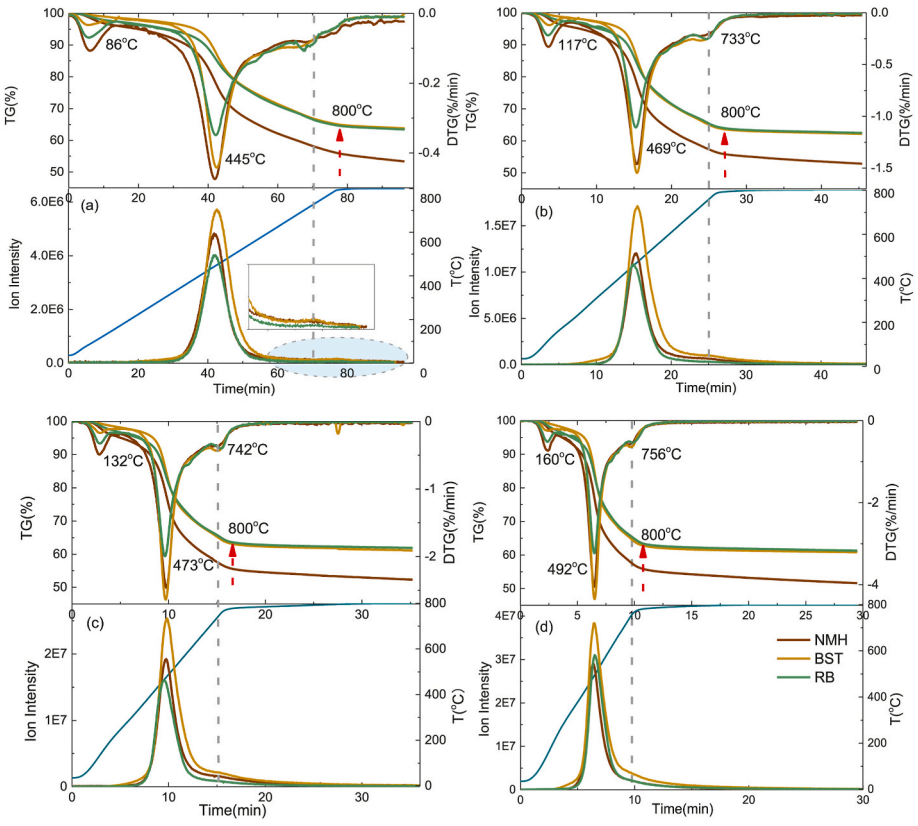

Fig. 2. TG-DTG curve and TIC curve (a) 10 °C/min, (b) 30 °C/min, (c) 50 °C/min, (d) 80 °C/min.

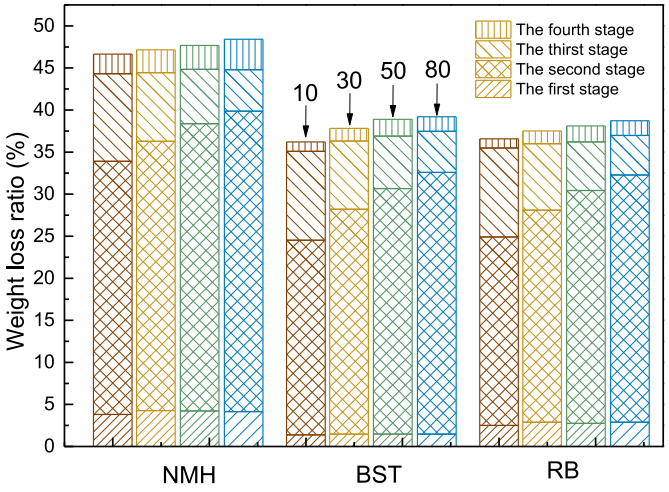

Fig. 3. The total mass loss and the mass loss of four stages at different HRs.

with 3~6 ring).

3. Results and discussion

3.1. TG-DTG and TIC analysis

In Fig. 2, as the HR increases, the position of the DTG peak gradually moves to higher temperatures, showing that HR affects the primary pyrolysis of coal. Moreover, the peak value of DTG increases greatly, suggesting the faster HR brings about a large amount of energy, which makes the volatiles release rapidly. The pyrolysis process is divided into drying stage, pyrolysis stage, polycondensation stage, and isothermal pyrolysis stage. The first stage involves the release of H_2O and CO_2 and corresponds to the first DTG peak. The second stage mainly undergoes cracking reactions and the release of primary volatiles, corresponding to the second DTG peak. The third stage is dominated by polycondensation reactions, with the conversion of semi-coke to char, accompanied by cracking reactions, corresponding to the third DTG peak. The peak positions of the total ion current (TIC) curve and DTG curve are in one-to-one correspondence at different HRs. Furthermore, the presence of the second peak in the TIC indicates that tar is still produced during the polycondensation stage, and this peak is mainly attributable to PAHs from the following analyses.

It can be seen from Fig. 3 that the increased HR leads to a gradual rise in mass loss. Char is predominantly derived from the solid residue after coal pyrolysis, with a minor fraction derived from polycondensation reactions of volatiles [35]. The bonds break more rapidly than they rearrange under faster HR, facilitating the release of volatiles. As the residence time of the volatiles in the particle decreases with increasing HR, the reactions between the volatile radicals and the solid radicals are reduced, thus reducing the char. The mass loss of NMH is much greater than that of BST and RB, which is related to the volatile content in the coal. While NMH has the highest volatile content, its TIC peak intensity is lower than that of BST, which is related to the coal structure.

In Fig. 3, the mass loss of NMH during the first stage is greater than that of the other two coals. This is consistent with the DTG peak value. As the HR rises, the mass loss ratio of three coals in the second stage increases, showing the release of a large amount of primary volatiles, which explains the elevation in the first peak intensity of 1~2 ring aromatics in the subsequent text. In the fourth stage, the mass loss of coal increases with HR. This is attributed to a higher degree of graphitization of the char at slow HR, resulting in increased resistance to volatile release and reduced mass loss during the isothermal stage. This explains why the second peak intensity of TAHs and PAHs enhances with the HR in the following section. To verify the above conjecture, the ^{13}C NMR and XRD analyses are presented below.

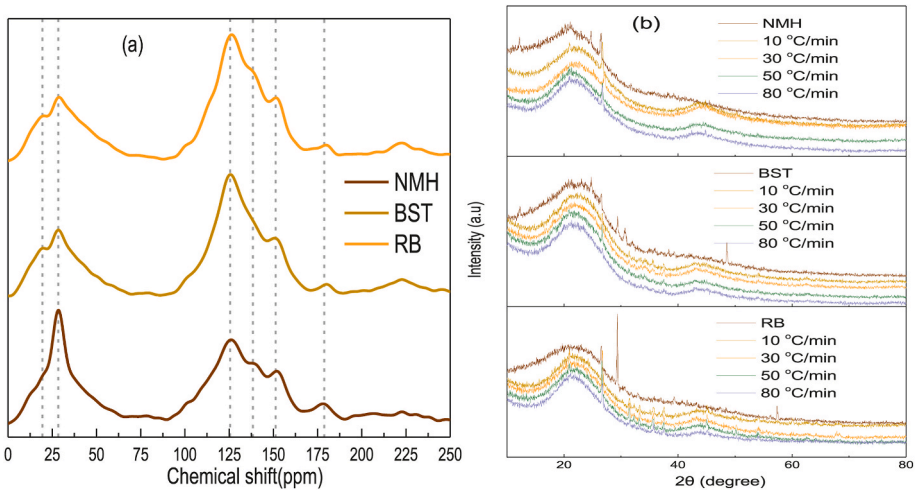

Fig. 4. (a)^{13}C NMR spectra of three coals and (b)XRD spectra of char at different HRs.

Table 3
Chemical shift values and relative contents of the different carbon types in solid^{13}C NMR spectra.

Symbols	Structural fragments	Chemical shift	Relative content/%		
			NMH	BST	RB
f_{al}^{3}	aliphatic CH_3	14~16	3.28	2.94	3.2
f_{al}^{a}	aromatic CH_3	16~22	5.97	6.95	5.63
f_{al}^{2}	methylene	22~36	16.72	11.86	8.97
f_{al}^{1+*}	methine, quaternary	36~50	9.08	9.17	9.61
f_{al}^{O}	oxy-aliphatic carbon	50~90	5.78	1.83	4.26
f_{ar}^{H}	aromatic protonated	100~129	23.86	28.59	25.19
f_{ar}^{B}	aromatic bridgehead	129~137	7.5	12	12.81
f_{ar}^{S}	aromatic branched	137~148	12.16	11.07	13.87
f_{ar}^{O}	oxy-aromatic carbon	148~165	7.73	10.68	11.17
f_{a}^{CC}	carboxyl carbon	165~180	3.83	1.27	2.23
f_{a}^{CC}	carbonyl carbon	180~220	4.09	3.53	3.06
Symbols	Significance	Expression			
f_{al}	aliphatic carbon	$f_{al}=f_{al}^{3}+f_{al}^{a}+f_{al}^{2}+f_{al}^{1+*}+f_{al}^{o}$	40.83	32.75	31.67
f_a	aromatic carbon	$f_a=f_{ar}^{H}+f_{ar}^{B}+f_{ar}^{S}+f_{ar}^{O}$	51.25	62.34	63.04
δ	the degree of aromatic substitution	$\delta=(f_{ar}^{B}+f_{ar}^{c}+f_{ar}^{o})/f_a$	0.53	0.54	0.60
X_b	the degree of condensation of the aromatic structure	f_{ar}^{B}/f_a	0.15	0.19	0.20
CH_2/CH_3			1.81	1.20	1.02

3.2. The ^{13}C NMR of coal and the XRD analysis of char

The carbon structure in low-rank coal is analyzed by solid-state ^{13}C NMR. Fig. 4(a) exhibits the solid-state ^{13}C NMR spectra of three coals. According to the literature, carbon types in coal are classified as aliphatic units, aromatic units and carbonyl units [36]. The chemical shifts corresponding to the peak areas are listed in Table 3. Peak-Fit software is employed to perform the peak-fitting process to obtain 14 carbon structural parameters [36]. The results are shown in Table 3. A high CH_2/CH_3 ratio is associated with increased gas production [37]. NMH has the highest CH_2/CH_3 ratio, consequently resulting in the highest percentage of gases in its volatiles. NMH and RB contain more f_{al}^{O} and f_a^{CC} than BST, which indicates that NMH and RB produces more CO_2 and H_2O than BST. The δ represents the degree of aromatic substitution [38]. The δ values for NMH, BST, and RB are 0.53, 0.54, and 0.6, respectively, indicating an average of 3, 3, and 4 substituents on each aromatic ring. The high proportion of PHs can be attributed to the high ratio of f_{ar}^{O} and f_{ar}^{B}. X_b is used to characterize the degree of condensation of the aromatic structure [38]. The X_b values for NMH, BST, and RB are 0.15, 0.19, and 0.2, respectively. The value of X_b for naphthalene is 0.2, so each cluster possesses on average 2-ring aromatic structures in BST and RB, while NMH is dominated by 1~2-ring aromatic structures. BST and RB have larger aromatic clusters than NMH.

The degree of graphitization of the char is analyzed by the XRD

Table 4
The structural parameters of char at different HRs.

Coal	HR (°C/min)	002 peak (2θ)	d_{002}
NMH	10	24.56	3.63
	30	24.34	3.66
	50	23.97	3.72
	80	23.75	3.75
BST	10	24.51	3.64
	30	24.38	3.65
	50	24.22	3.68
	80	24.03	3.71
RB	10	24.40	3.65
	30	24.27	3.67
	50	24.18	3.68
	80	23.89	3.73

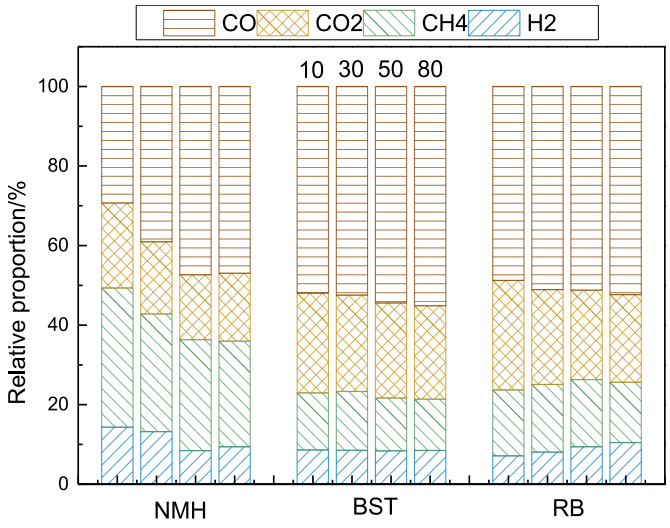

Fig. 5. The relative proportions of four main gases under different HRs.

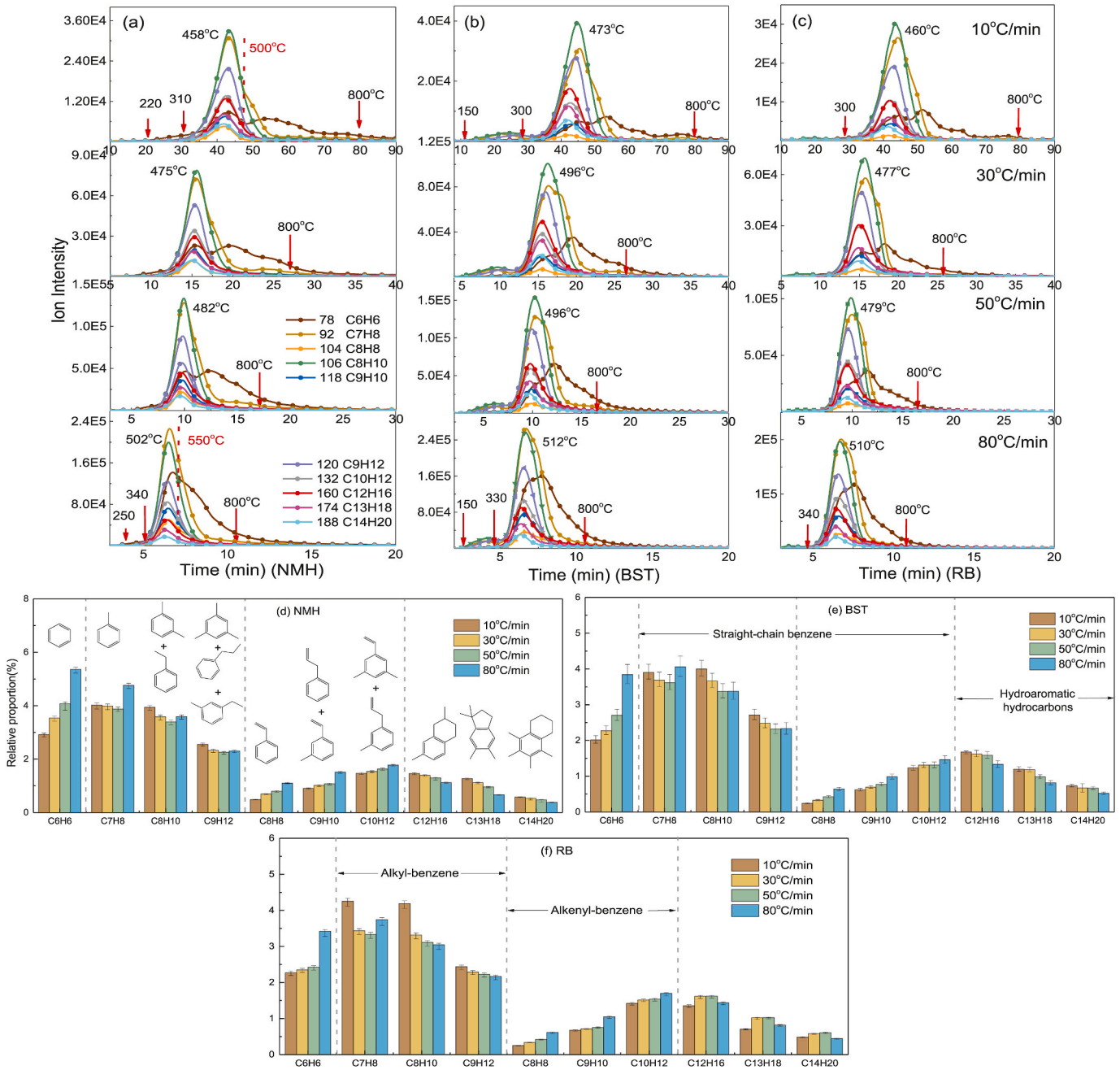

Fig. 6. Variation of evolution curves of MAHs versus HR (a) NMH, (b) BST, (c) RB; Variation of the relative proportion of MAHs versus HR (d) NMH, (e) BST, (f) RB.

pattern. It can be seen from Fig. 4(b) that there are two sharp peaks at approximately 23° and 43°, representing the (002) band and the (100) band, respectively. As the HR increases, the (002) band changes less, whereas the (100) band diminishes, implying a reduction in graphitization of the char [39]. To demonstrate clearly the variation in the graphitization degree of char, the microcrystalline structure parameters are calculated and presented in Table 4. As the HR increases, the (002) band gradually shifts towards poorer graphitization and the d_{002} value gradually increases, suggesting the degree of graphitization of char gradually decreases.

3.3. The relative proportions of gas products

Fig. S2 displays the gas release curves. As HR rises, the peak shifts to higher temperatures, and the peak intensity increases. Additionally, the gas release curves show that the intensity of NMH is higher than that of BST and RB. Fig. 5 shows the relative proportions of gases. As HR increases, the relative proportions of CO produced by NMH and BST pyrolysis elevate, while those of H_2 decline. The increase in CO proportion at fast HR can be attributed to the decomposition of oxygenated compounds in primary volatiles [40,41]. However, the relative proportion of H_2 produced by RB pyrolysis increases slightly with HR, which is related to the higher hydrogen content in RB.

3.4. The evolution characteristics of main tar compounds

3.4.1. The online evolution curves of MAHs

The evolution curves of the MAHs are shown in Fig. 6(a~c). For NMH, at 10 °C/min, the initial release temperature of benzene exhibits approximately 220 °C, while that of other MAHs are at around 310 °C. For BST, there is a weak peak of alkyl-benzene between 150 and 300 °C. For three coals, the evolution curves of MAHs reach their maximum

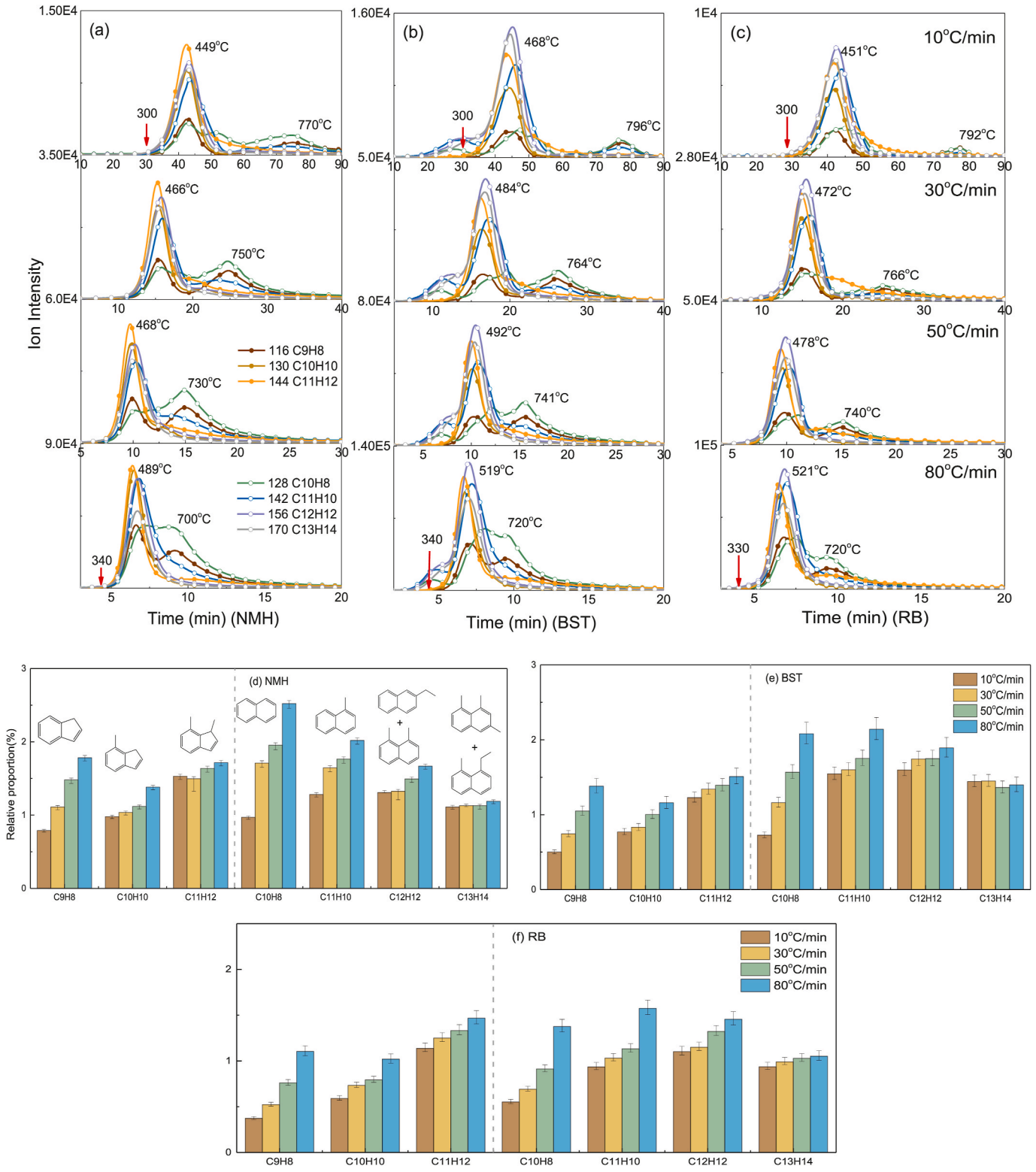

Fig. 7. Variation of evolution curves of BAHs versus HR (a) NMH, (b) BST, (c) RB; Variation of the relative proportion of BAHs versus HR (d) NMH, (e) BST, (f) RB.

value at 460–475 °C, and MAHs with longer alkyl side chains end earlier. There are two pathways for the formation of volatiles: primary pyrolysis of coal, and secondary reactions of primary volatiles or continuous pyrolysis of coal at higher temperatures [14]. Therefore, the evolution curves of some MAHs exhibit double peaks, such as benzene and toluene. The first peak corresponds to the primary pyrolysis of the coal, while the second peak is mainly associated with the polycondensation of semi-coke and the continuous cleavage of covalent bonds. Throughout the pyrolysis process, the primary volatiles undergo secondary reactions, which are more probable to occur at temperatures above 500 °C.

As the HR increases, the initial, maximum and ending points of the MAHs all shift towards higher temperatures. Coal pyrolysis is an endothermic reaction [42]. As the HR increases, the temperature of reactor rises rapidly, but the heat does not penetrate coal particles quickly

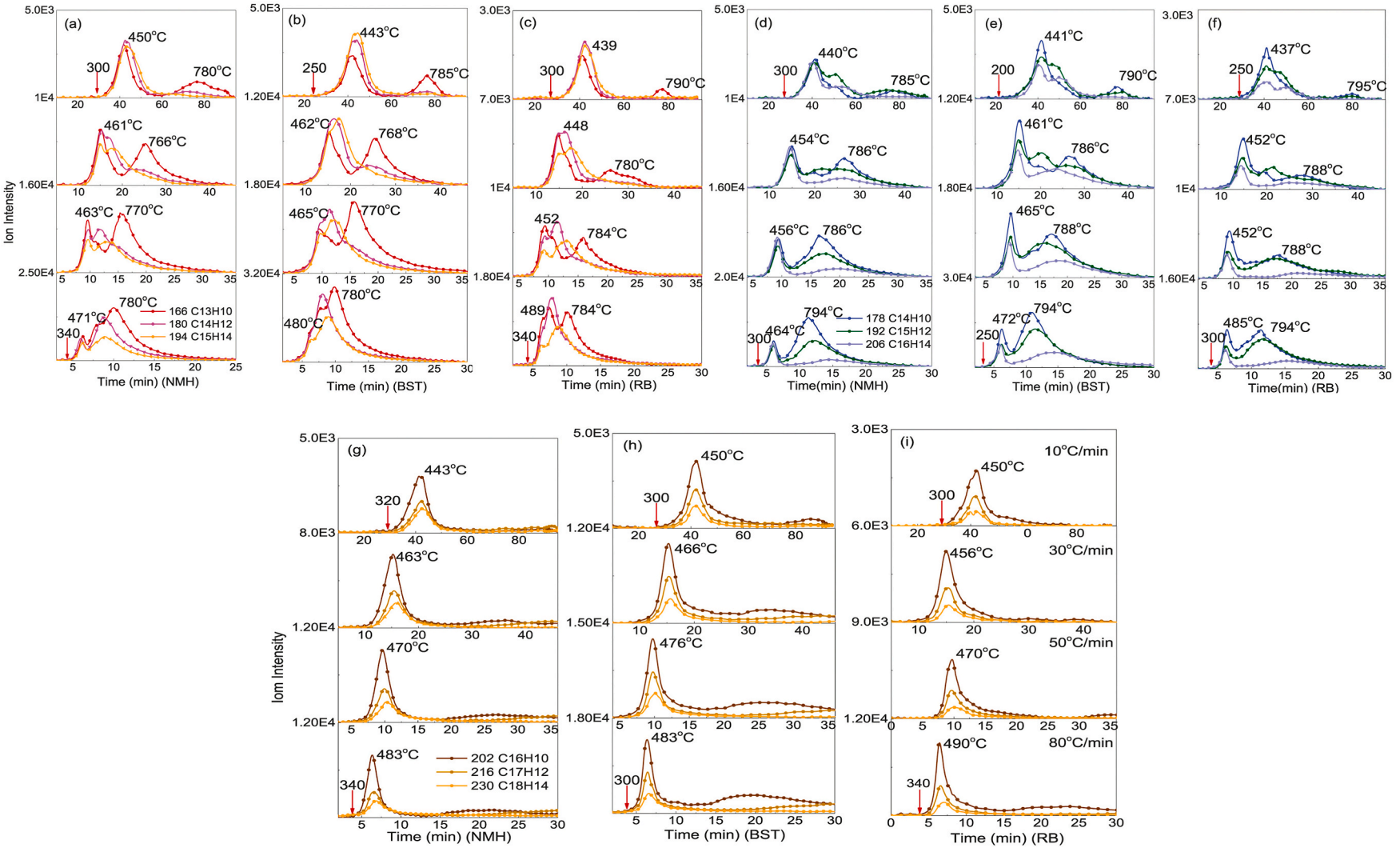

Fig. 8. Variation of evolution curves of PAHs with the HR (a~c) Fluorene series, (d~f) Phenanthrene series, (g~i) Pyrene series.

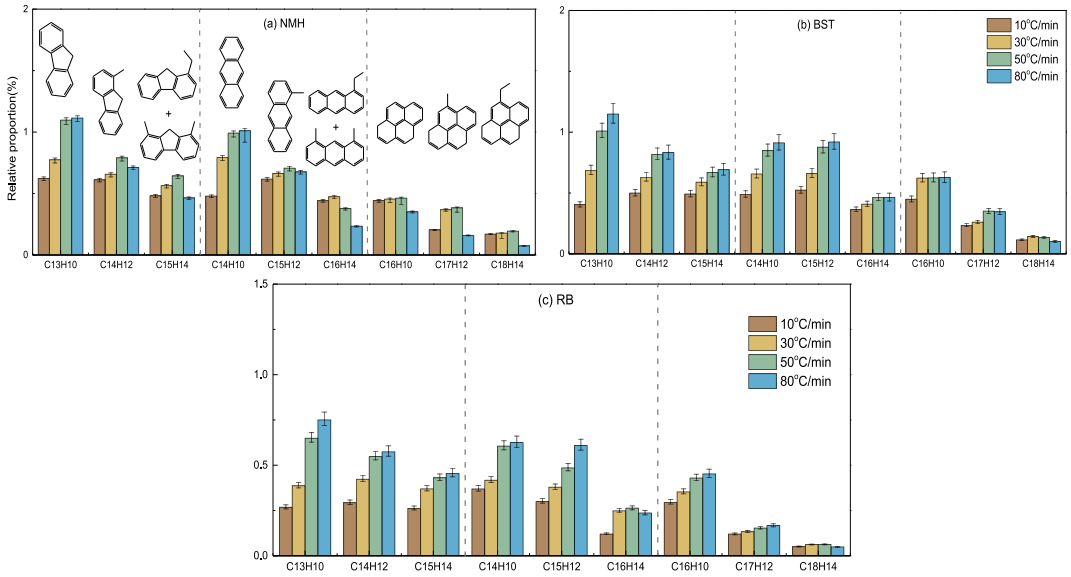

Fig. 9. Variation of the relative proportion of PAHs with the HR (a) NMH, (b) BST, (c) RB.

enough, resulting in a time lag in the evolution peak. The higher the HR, the more pronounced the hysteresis, indicating that HR affects the pyrolysis of coal macromolecules themselves. For MAHs with two peaks, as the HR increases, the intensity of the first peak increases more significantly than that of the second peak. Additionally, the first peak lags behind while the second peak moves forward, with the two peaks gradually merging. This indicates that as the HR increases, the second peak of MAHs gradually originates from the secondary cracking of primary volatiles, while the proportion originating from the continuous pyrolysis of coal at higher temperatures diminishes. The amount of alkenyl-benzene produced by secondary reactions increases with increasing HR, causing a tailing at the end of the evolution curve. As the HR increases, the intensity of C_7H_8 gradually exceeds that of C_8H_{10} and the intensity of C_6H_6 increases significantly. In addition, the intensity of straight-chain benzene varies much more than that of hydroaromatic hydrocarbons with HR, so the proportion of hydroaromatic hydrocarbons tends to decrease. The relative proportions of the MAHs are depicted in Fig. 6(e~f).

For NMH and BST, the proportion of benzene and alkenyl-benzene increases, alkyl-benzene initially decreases and then increases, and hydroaromatic hydrocarbons declines. The variation in hydroaromatic hydrocarbons in RB may be related to its H content. At slow HR, the proportion of benzene is smaller than that of alkyl-benzene, but with the increasing HR, the proportion of benzene gradually exceeds that of alkyl-benzene, further verifying the enhanced secondary cracking of primary volatiles. The faster HR firstly promotes primary pyrolysis of coal to generate more alkyl-benzene, but also accelerate the breaking of the side chains of alkyl-benzene. The competing reactions of the two determine the final proportion of alkyl-benzene. The proportion of toluene increases considerably at 80 °C/min due to the accelerated release of toluene during primary pyrolysis.

3.4.2. The evolution curves of BAHs

The evolution curves of BAHs are shown in Fig. 7(a~c). Coal has a two-phase physical structure, a stationary phase and a mobile phase. The former is linked by covalent bonds, while the latter is linked by non-covalent bonds [32]. For BST, at 10 °C/min, the evolution curves of naphthalene series compounds show a peak around 180–300 °C, which is due to the cleavage of non-covalent bonds. The initial points of the BAHs for the NMH and RB are around ~300 °C.

The higher HR increases the temperature difference between the inside and outside of the coal particles, resulting in the enhancement of instantaneous energy impact and the fracture of side chains and functional groups [27]. The second peak of BAHs increases with increasing HR, and the second peak shifts forward instead of lagging behind, suggesting that it is gradually generated from the secondary cleavage of primary volatiles. The higher the HR, the greater the degree of the secondary cracking of primary volatiles, including dehydrogenation of cyclic compounds, dehydroxylation of PHs, debranching of aromatics, cleavage of polycyclic aromatics and aromatization of long-chain aliphatic hydrocarbons. At the slow HR, these reactions are unlikely to occur, so the second peak of BAHs is mainly derived from the pyrolysis of coal in the polycondensation stage. It can be seen from section 3.1 that the weight loss in the polycondensation stage decreases with the HR. This shows that as the HR increases, the second peak of BAHs progressively originates from the secondary cracking of primary volatiles, while the proportion originating from coal continuous pyrolysis at higher temperatures decreases. At 10 °C/min, the intensity of the first peak is greater than that of the second peak, indicating that more MAHs and BAHs are generated from the coal primary pyrolysis. As the HR increases, the first peak increases more than the second peak, indicating that the coal primary pyrolysis still produces more MAHs and BAHs than the secondary pyrolysis of primary volatiles.

The proportions of BAHs are shown in Fig. 7(e~f). The relative proportions of BAHs gradually increase as the HR rises. The basic units of low-rank coal are mainly composed of 1~2 ring aromatics, whereas higher HR accelerates the cleavage of the coal macromolecular structure and primary volatiles, thus increasing the proportion of BAHs. The relative proportions of the stable BAHs (indene and naphthalene) gradually exceeds those of other BAHs, indicating that as the HR increases, other BAHs transform into indene and naphthalene.

3.4.3. The evolution curves of PAHs

The PAHs evolution curves are shown in Fig. 8. As the HR rises, the variations in the evolution curves of PAHs differ from those of MAHs and BAHs. For fluorene series (shown in Fig. 8(a~c)), there are two distinct peaks at 10 °C/min. With increasing HR, the number of peaks first increases and then decreases, with 50 °C/min being the turning point. When the HR is below 50 °C/min, the increased HR promotes secondary cleavage of primary volatiles, resulting in an increase in precursors of fluorene series and a corresponding growth in the number of peaks. As the HR increases to 80 °C/min, the secondary cracking of each precursor occurs simultaneously and the interval between peaks becomes less pronounced. For phenanthrene series (shown in Fig. 8(d~f)), the

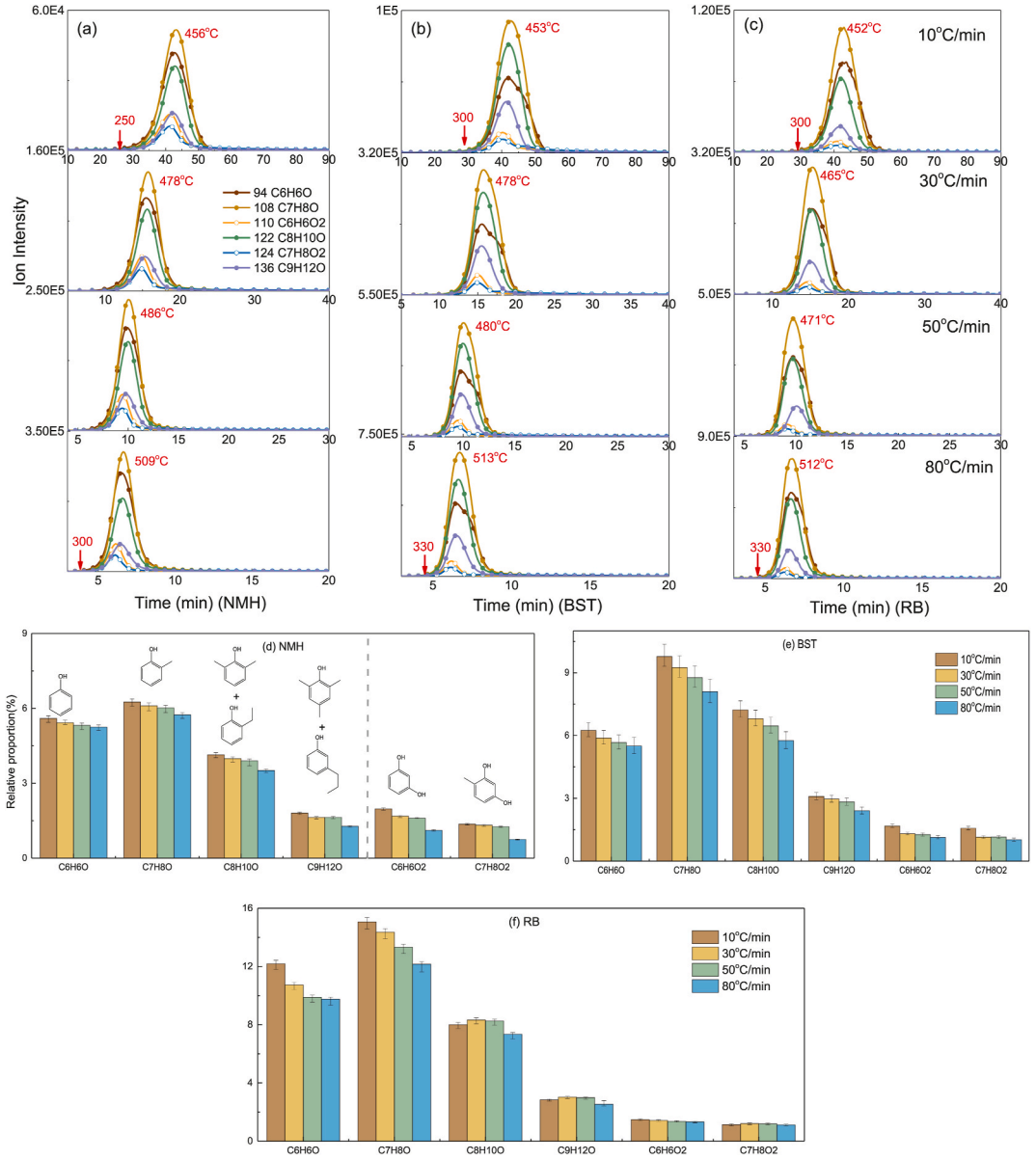

Fig. 10. Variation of evolution curves of the PHs with the HR (a) NMH, (b) BST, (c) RB; Variation of the relative proportion of PHs with the HR (d) NMH, (e) BST, (f) RB.

number of peaks decreases as the HR increases, with only two major evolution peaks at 80 °C/min. This is because the precursors of phenanthrene series have their own specific decomposition peaks in a certain temperature range. If the HR is low enough, most of these peaks can occur individually during pyrolysis process. However, some of these peaks decompose simultaneously at higher HR. For pyrene series, the second peak gradually appears with the increase of HR.

It is reported that PAHs are mainly derived from coal pyrolysis at low temperature and secondary reactions at high temperature [32]. Therefore, the first peak of PAHs is attributed to coal pyrolysis while the source of second peak above 550 °C is related to the HRs. Heating to the same temperature with a slow HR provides more time for coal to decompose into gases and liquids. Therefore, at slow HR, the second peak of PAHs are mainly attributed to the continuous pyrolysis of coal at higher temperatures. As the HR increases, the covalent bonds of coal break more quickly, as well as the cleavage of primary volatiles intensifies. The heavy PAHs (>4 ring) in the volatiles are cleaved to form small PAHs, and the dehydrogenation of the hydrogenated benzene and the aromatization of the aliphatic hydrocarbons into small PAHs enhance. It shows that continued pyrolysis of coal at higher temperatures and secondary cracking of primary volatiles are the major reasons for the increase in the total content of PAHs. It is worth that the increase in the second peak for RB coal is less than that for NMH and BST coal. In conjunction with Section 3.4.1, it is clear that there is less hydroaromatic hydrocarbons converted to PAHs for RB coal. As the HR increases, the position of the second peak does not shift forward with the HR. Combining the mass loss peak at polycondensation stage on the DTG curve with the second peak of the TIC in one-to-one correspondence, it can be concluded that under faster HR, the second peak is gradually generated by the continued pyrolysis of coal at higher temperatures. As the HR increases, the intensity of second peak is strengthened. However, the first peak for certain PAHs decreases with HR, which is because the concentrated energy promotes cleavage reactions and is the reason why the first peak of MAHs and BAHs greatly enhances. At 10 °C/min, the intensity of first peak is greater than that of second peak from the evolution curve throughout the pyrolysis process, indicating that more PAHs are produced by coal primary pyrolysis. As the HR rises, the increase of first peak is much smaller than that of second peak, indicating

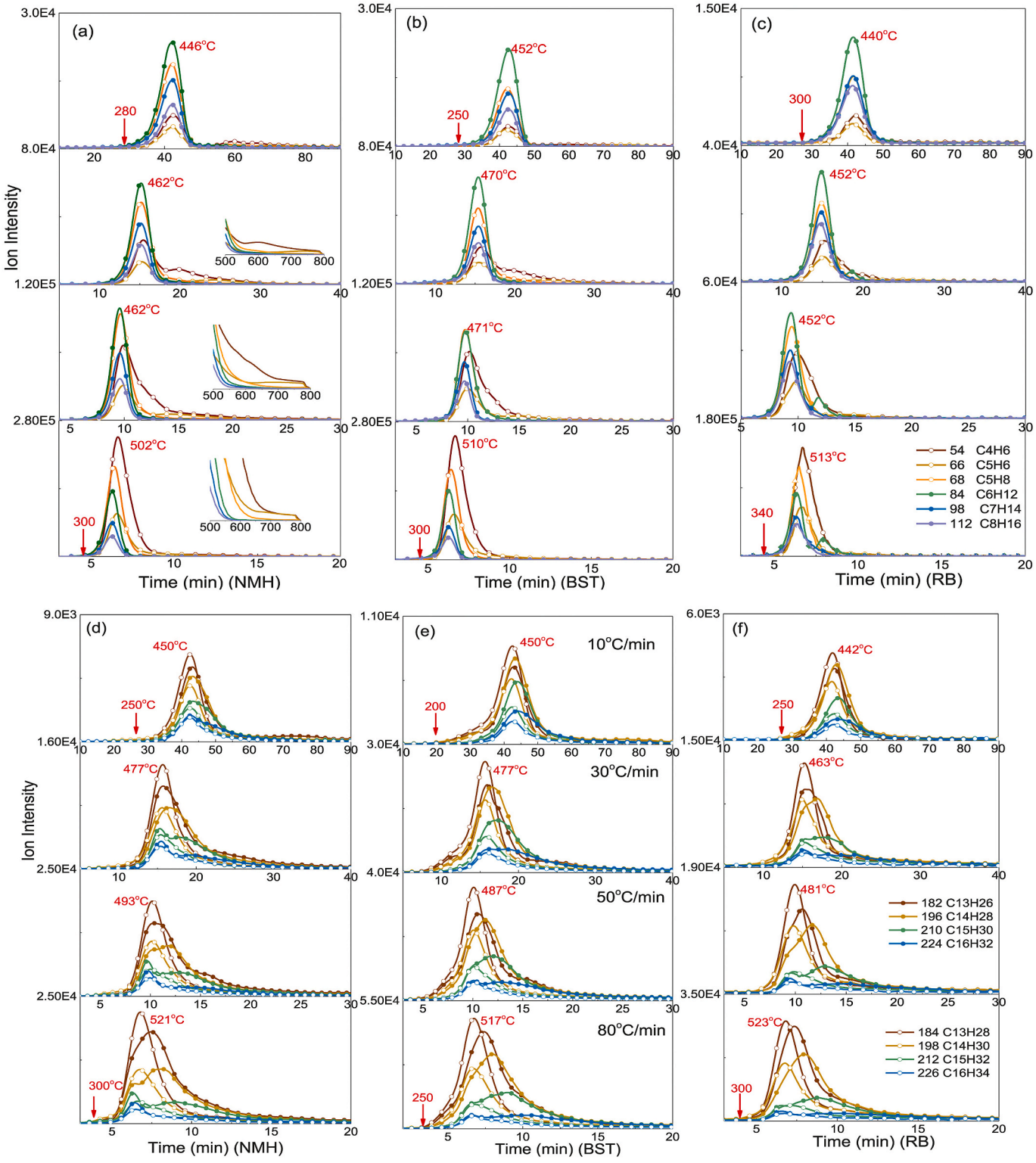

Fig. 11. Variation of the evolution curves of the aliphatic hydrocarbons with the HR (a~c) C4–C10, (d~f) C11–C19.

that the continuous pyrolysis of coal at higher temperatures is the major reason for the increase in the total PAHs content, and the second peak produces more PAHs than the first peak (except pyrene series).

The proportions of PAHs are shown in Fig. 9. As the HR increases, the proportion of PAHs with $m/z < 190$ increases for three coals. However, for NMH, the proportion of PAHs with $m/z > 190$ increases and then decreases, while the other two coal continue to increase. This may be due to the larger size of aromatics that make up the basic network structure of the BST and RB macromolecules according to ^{13}C NMR.

3.4.4. *The evolution curves of phenolic compounds*

In Fig. 10(a~c), there is only one peak on the evolution curves of phenolic compounds (PHs) throughout the pyrolysis process. At 10 °C/min, PHs are released in the range of 300~600 °C, reaching a maximum at ~450 °C. As the HR increases, the evolution curves overall lag behind.

The proportion of PHs is depicted in Fig. 10(e~f). The formation of

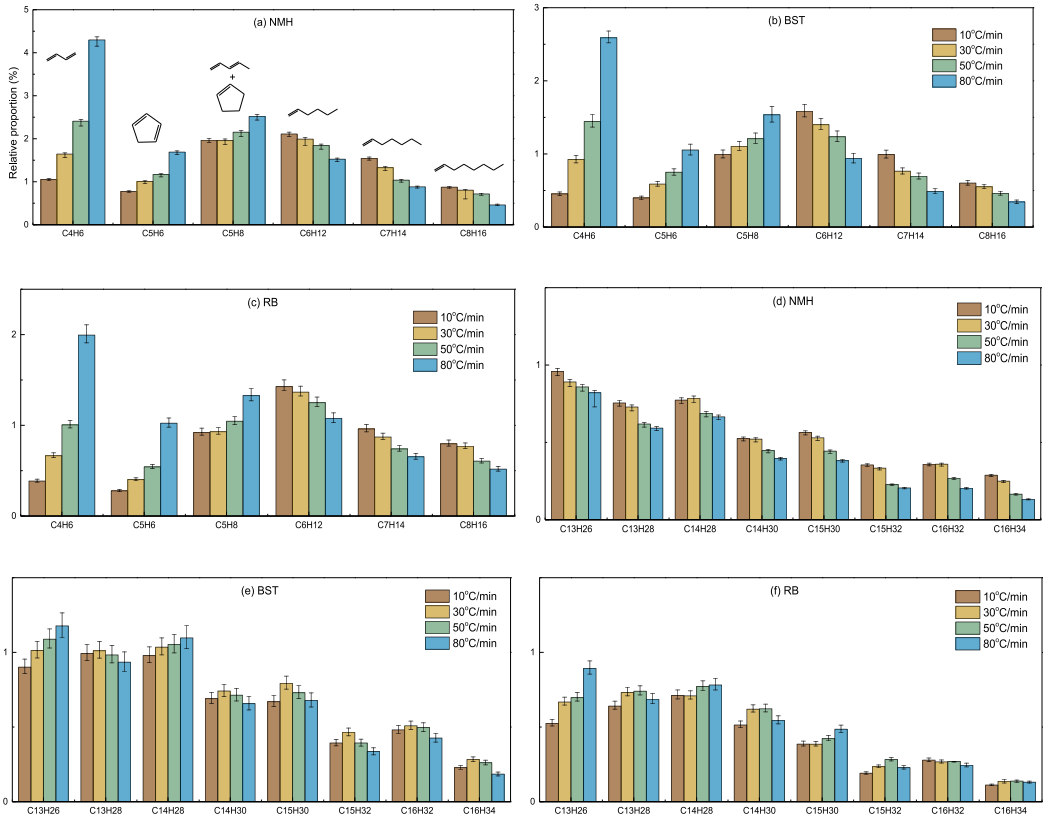

Fig. 12. Variation of the relative proportion of aliphatic hydrocarbons with the HR (a~c) C4–C10, (d~f) C11–C19.

PHs is closely related to the type of free radical e.g. ·H or $\cdot CH_3$ and the chemical structure of oxygenated aromatic carbon during pyrolysis process [32,43]. The peaks within 150~165 ppm on the ^{13}C NMR spectrum correspond to aromatic C═O, including phenolic carbon, methoxy carbon and aromatic ether carbon. Based on ^{13}C NMR results, the largest content of f_a^O in RB results in the highest ratio of PHs in RB. The proportion of PHs in NMH and BST gradually decreases with increasing HR, while the changes of PHs in RB are more complex but show an overall decreasing trend, suggesting that the higher HR promotes the dehydroxylation of PHs to generate aromatic radicals, which in turn are converted into aromatics and more oxygen enter into the gas.

3.4.5. *The evolution curves of aliphatic hydrocarbons*

In Fig.11, the temperature at which the evolution curve of C4–C10 reaches its maximum value coincides with that of TIC, the release in this temperature range being attributed to the primary pyrolysis of coal. There is no clear pattern in the ending time of C4–C10 at 10 °C/min. Whereas the ending time of C4–C10 follows the order of alkenes < dienes at 80 °C/min. As the HR increases, the peak intensity of C4–C10 increases, but it is noteworthy that the evolution curves of the alkenes, excluding the dienes, exhibit a single peak. Therefore, this study discusses dienes and alkenes separately. From 50 to 80 °C/min, there is no significant increase in alkenes. On the one hand, higher HR promotes the primary pyrolysis of coal, leading to the release of large amounts of volatiles and an increase in alkenes. On the other hand, higher HR promotes the conversion of alkenes into dienes. The competition between these two reactions results in no significant increase in the intensities of alkenes. As the HR increases, the maximum of alkenes remains lagging, while the ending point slightly advances. The curves of dienes show tailing and end later than alkenes.

The release of C11–C19 starts earlier and ends later compared to C4–C10. It indicates that pyrolysis initiates with the cracking of weak bonds in coal. The longer aliphatic hydrocarbons have lower bond energies and easier to break. While the condensation stage of coal pyrolysis is dominated by the release of macromolecular tar, so the release time of C11–C19 is longer than that of C4–C10 in the whole pyrolysis process. As the HR rises, the ending time of long-chain alkenes gradually delays. At 80 °C/min, the long-chain alkenes obviously end later than the long-chain alkanes, indicating that the increased HR promotes the conversion of alkanes to alkenes. When the HR increases from 30 to 80 °C/min,

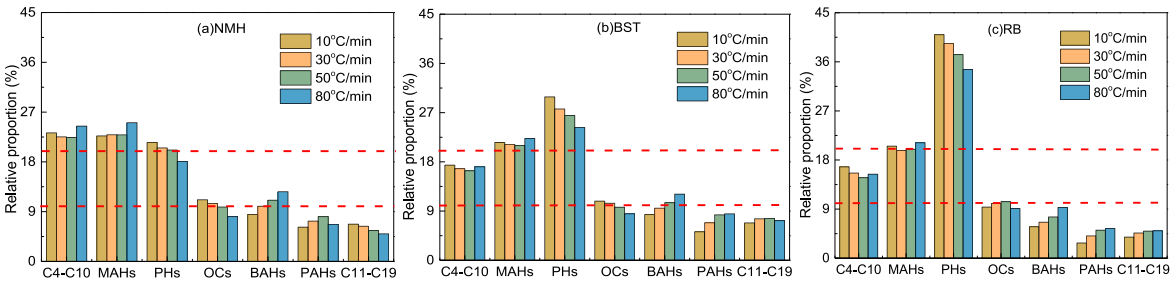

Fig. 13. Variation of the proportion of components in tar with the HR (a) NMH, (b) BST, (c) RB.

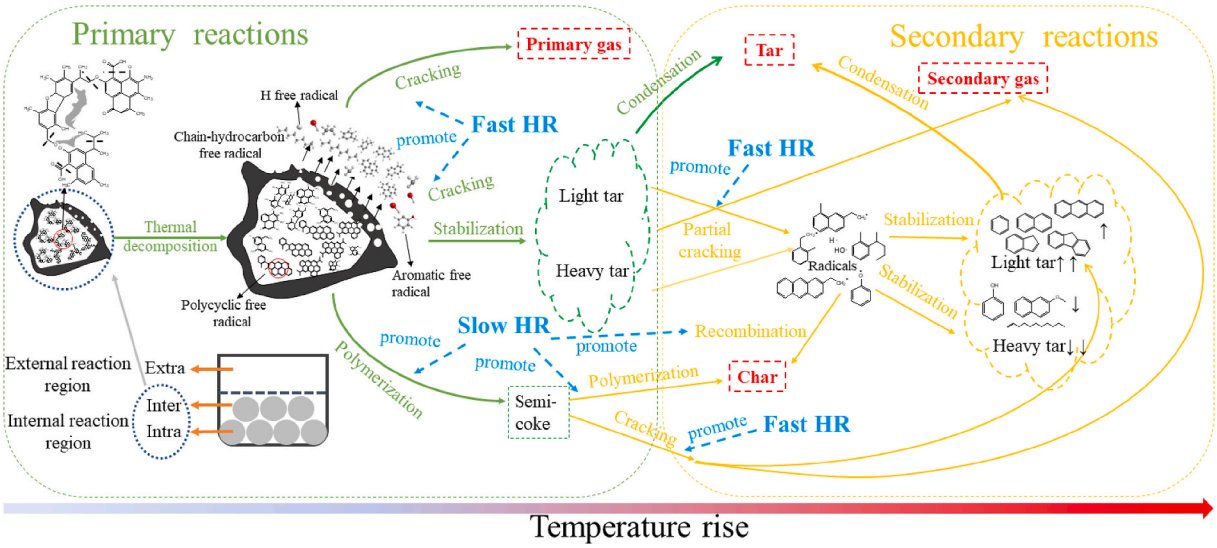

Fig. 14. The pyrolysis mechanism of low-rank coal at different HRs.

the peak intensity of C11–C19 in NMH does not increase significantly. Additionally, the peak intensity of $m/z > 200$ decreases. However, for BST and RB, the peak intensity of C11–C19 has been gradually increasing with the HR.

According to Fig.12, the proportion of aliphatic hydrocarbons varies among different coal types, with NMH having a greater proportion of C4–C10 compared to BST and RB. For three coals, as the HR increases, there is a significant decrease in the proportion of alkenes and a considerable increase in dienes. The ^{13}C NMR results indicate that the proportion of f_{al} in the NMH and BST is greater, resulting in a higher proportion of C11–C19 compared to RB. The aliphatic structures in coal are covalently bonded as bridges and side chains on aromatics or cross-linked to the macromolecular structure in the free state in the coal structure. These different forms of existence result in varying changes in the proportion of C11–C19 among the three coals as the HR increases.

3.5. The mechanism of heating rate on coal pyrolysis

The proportions of the components in the tar are shown in Fig. 13. NMH has the highest f_{al} content, which results in the highest concentration of aliphatic hydrocarbons (ALHs) than the other two coals. BST and RB have a higher f_{ar}^{O} content, resulting in a greater proportion of PHs compared to NMH. On the contrary, NMH has a higher f_{al}^{O} content, facilitating the transfer of oxygen to H_2O and CO_2.

As the HR increases, the secondary cracking reactions of primary volatiles in the interior enhance, resulting in the decomposition of PHs, OCs, ALHs, and macromolecular compounds, producing free radicals. These free radicals form more stable aromatics through free radical recombination or Diels-Aldertype reactions, promoting cyclization and aromatization reactions [40,44]. Li et al. observed secondary reactions between the volatile fragments outside the particles, thus leading to an increase in the content of PHs [29]. In this work, the secondary reactions of volatiles outside the particle are inhibited. Consequently, for the three coals, as the HR increases, the proportions of PHs and OCs decrease, and the proportion of light aromatics (<4 ring) increases, the proportions of C4–C10 and MAHs initially decrease and then increase, and the dienes and benzene increase significantly. This is because the increased HR promotes primary pyrolysis of the coal and secondary cracking of the volatiles. The large release of primary volatiles results in significant tar production, while secondary cracking consumes alkenes and aromatics with side chains. Thereby the final proportion is determined by the two reactions of production and consumption.

For NMH, as the HR increases, the proportion of PAHs initially rises and then declines. It is clear from section 3.4.3 that the increase in PAHs in the range of 10~50 °C/min is mainly attributed to the increase in fluorene, phenanthrene and pyrene. When the HR reaches 80 °C/min, both peaks of certain PAHs are reduced by cleavage into smaller cyclic molecules, ultimately resulting in a decrease in the total proportion of PAHs. The proportion of C11–C19 decreases with increasing HR, mainly due to enhanced secondary reactions of primary volatiles. The types and quantities of PAHs generated during coal pyrolysis are closely related to the contents of f_{ar}^{H} and f_{ar}^{B} in coal [37]. BST and RB are more mature than NMH, with more heavy components in the tar after pyrolysis, and the competing reactions of generation and consumption ultimately lead to an increase in PAHs and C11–C19.

In conclusion, the increase in HR improves the content of primary volatiles by enhancing the primary cracking reaction of coal, and also promotes the secondary cracking and aromatization of primary volatiles, resulting in a higher proportion of light components and light aromatics in the tar. An increased HR inhibits the polycondensation reaction throughout the pyrolysis process, thereby reducing the char yield and the proportion of heavy components in the tar. Despite variations in coal types, macromolecular structures are similar and the mechanism of HR on the covalent bond breaking remains consistent. This means that the breakage of covalent bonds in the coal pyrolysis process follows a certain regulation. Hence, as HR increases, the evolution curve and proportion of tar components exhibit similar trends across different coals. However, the content of each component in the tar varies due to the different elemental content of coals. The mechanism of HR on the pyrolysis of low-rank coal is shown in Fig. 14.

4. Conclusion

In this work, the effects of HR on the product distribution of in-situ tar and online evolution curves of volatiles for the pyrolysis of low-rank coals were investigated. The escape pattern of volatiles was obtained from the real-time evolution curves, then the influence of HR on the internal secondary reaction was analyzed, the association between reaction products and molecular structures was constructed, and finally the pyrolysis mechanism was deduced. As the HR increases, the peak value of DTG increases significantly, indicating the release rate of primary volatiles is greatly accelerated. The peak positions appearing on the TIC profile well correspond to those on the DTG profile, and hysteresis also occur. ALHs (except dienes), PHs, and OCs have only one evolution peak, while dienes and aromatics have one or more evolution peaks throughout the pyrolysis process. The first peak is attributed to the

coal primary pyrolysis, and the second peak belongs to the secondary cracking of volatiles and the continued pyrolysis of coal at higher temperatures. At slow HR, the second peak for aromatics is mainly attributed to the pyrolysis of coal. As the HR rises, the second peak for MAHs and BAHs are mainly derived from the cracking of primary volatiles, and the second peak for PAHs from the continued cracking of coal at higher temperatures. At slow HR, aromatics are mainly derived from the primary pyrolysis of coal. As the HR increases, MAHs and BAHs are still mainly produced by the primary pyrolysis of coal, but the increase in PAHs is mainly attributed to the continuous pyrolysis of coal at higher temperatures. As the HR increases, the proportion of PHs and OCs decreases, that of aromatics increases and ALHs varies slightly for different samples. Overall, the HR increases the yield of primary volatiles by enhancing the primary cracking of coal, increase the proportion of light components and light aromatics in tar by promoting the internal secondary cracking and aromatization of the primary volatiles, reduce the yield of char and the proportion of heavy components in the tar by inhibiting the condensation reactions throughout the pyrolysis process. Because of the similar macromolecular structures of different coals, the evolution curve of different coals versus HRs follows a common law. Whereas, due to the different elemental contents of different coals, eventually leading to different proportions of tar components.

CRediT authorship contribution statement

Yao Zhu: Conceptualization, Data curation, Formal analysis, Investigation, Methodology, Validation, Writing – original draft, Writing – review & editing. **Qinhui Wang:** Conceptualization, Funding acquisition, Methodology, Project administration, Resources, Writing – review & editing. **Jiqing Yan:** Investigation, Writing – review & editing. **Jianmeng Cen:** Funding acquisition, Project administration, Resources, Supervision. **Mengxiang Fang:** Writing – review & editing, Supervision.

Declaration of competing interest

The authors declare that they have no known competing financial interests or personal relationships that could have appeared to influence the work reported in this paper.

Data availability

The data that has been used is confidential.

Acknowledgements

This research was financially supported by the Fundamental Research Funds for the Central Universities (2022ZFJH004).

Appendix A. Supplementary data

Supplementary data to this article can be found online at https://doi.org/10.1016/j.energy.2024.131183.

References

[1] Wang S, Tang X, Wang J, Zhang B, Sun W, Höök M. Environmental impacts from conventional and shale gas and oil development in China considering regional differences and well depth. Resour Conserv Recycl 2021;167:105368.
[2] Zhu Y, Wang Q, Yan J, Cen J, Fang M, Ye C. Influence and action mechanism of pressure on pyrolysis process of a low rank Naomaohu coal at different temperatures. J Anal Appl Pyrol 2022;167:105682.
[3] Ban Y, Jin L, Liu F, Zhu J, Li Y, Yang H, et al. Pyrolysis behaviors of model compounds with representative oxygen-containing functional groups in coal over calcium. Fuel 2022;310:122247.
[4] Wang P, Jin L, Liu J, Zhu S, Hu H. Analysis of coal tar derived from pyrolysis at different atmospheres. Fuel 2013;104:14–21.
[5] Wu Y, Zhu J, Zhao S, Wang D, Jin L, Hu H. Co-pyrolysis behaviors of low-rank coal and polystyrene with in-situ pyrolysis time-of-flight mass spectrometry. Fuel 2021;286:119461.
[6] Czech H, Sippula O, Kortelainen M, Tissari J, Radischat C, Passig J, et al. On-line analysis of organic emissions from residential wood combustion with single-photon ionisation time-of-flight mass spectrometry (SPI-TOFMS). Fuel 2016;177:334–42.
[7] Wang Y, Zhu Y, Zhou Z, Yang J, Pan Y, Qi F. Pyrolysis study on solid Fuels: from conventional analytical methods to synchrotron vacuum ultraviolet photoionization mass spectrometry. Energy Fuel 2016;30(3):1534–43.
[8] He W, Liu Z, Liu Q, Ci D, Lievens C, Guo X. Behaviors of radical fragments in tar generated from pyrolysis of 4 coals. Fuel 2014;134:375–80.
[9] Edinger P, Schneebeli J, Struis RPWJ, Biollaz SMA, Ludwig C. On-line liquid quench sampling and UV–Vis spectroscopy for tar measurements in wood gasification process gases. Fuel 2016;184:59–68.
[10] Wang Y, Liu C, Jia L, Peng Z, Wang J, Yang J, et al. On-line photoionization mass spectrometric study of the catalytic pyrolysis of acrylonitrile-butadiene-styrene copolymer over HZSM-5, HUSY and Al-MCM-41. Fuel 2022;307:121937.
[11] Zhang T, Zhang L, Hong X, Zhang K, Qi F, Law CK, et al. An experimental and theoretical study of toluene pyrolysis with tunable synchrotron VUV photoionization and molecular-beam mass spectrometry. Combust Flame 2009;156(11):2071–83.
[12] Jia L, Weng J, Wang Y, Sun S, Zhou Z, Qi F. Online analysis of volatile products from bituminous coal pyrolysis with synchrotron vacuum ultraviolet photoionization mass spectrometry. Energy Fuel 2013;27(2):694–701.
[13] Yang J, Wu Y, Zhu J, Yang H, Li Y, Jin L, et al. Insight into the pyrolysis behavior of polyvinyl chloride using in situ pyrolysis time-of-flight mass spectrometry: aromatization mechanism and Cl evolution. Fuel 2023;331:125994.
[14] Zhang X, Zhu J, Ban Y, Liu F, Jin L, Hu H. Effect of Fe_2O_3 on the pyrolysis of two demineralized coal using in-situ pyrolysis photoionization time-of-flight mass spectrometry. J Fuel Chem Technol 2021;49(5):589–97.
[15] Zhou Y, Li L, Jin L, Zhu J, Li J, Li Y, et al. Effect of functional groups on volatile evolution in coal pyrolysis process with in-situ pyrolysis photoionization time-of-flight mass spectrometry. Fuel 2020;260:116322.
[16] Zhu Y, Chen X, Wang Y, Wen W, Wang Y, Yang J, et al. Online study on the catalytic pyrolysis of bituminous coal over HUSY and HZSM-5 with photoionization time-of-flight mass spectrometry. Energy Fuel 2016;30(3):1598–604.
[17] Li S, Wang C, Luo Z, Zhu X. Investigation on the catalytic behavior of alkali metals and alkaline earth metals on the biomass pyrolysis assisted with real-time monitoring. Energy Fuel 2020;34(10):12654–64.
[18] Weng J-J, Liu Y-X, Zhu Y-N, Pan Y, Tian Z-Y. Online study on the co-pyrolysis of coal and corn with vacuum ultraviolet photoionization mass spectrometry. Bioresour Technol 2017;244:125–31.
[19] Li Y, Meng Q, Wang J, Zhang Y, Cao C, Cheng Z, et al. Experimental and theoretical investigation of the pyrolysis of furfural. J Phys Chem 2019;123(1):103–10.
[20] Zhu J, Yang H, Hu H, Zhou Y, Li J, Jin L. Novel insight into pyrolysis behaviors of lignin using in-situ pyrolysis-double ionization time-of-flight mass spectrometry combined with electron paramagnetic resonance spectroscopy. Bioresour Technol 2020;312:123555.
[21] Shi Z, Jin L, Zhou Y, Li H, Li Y, Hu H. In-situ analysis of catalytic pyrolysis of Baiyinhua coal with pyrolysis time-of-flight mass spectrometry. Fuel 2018;227:386–93.
[22] Mühlberger F, Streibel T, Wieser J, Ulrich A, Zimmermann R. Single photon ionization time-of-flight mass spectrometry with a pulsed electron beam pumped excimer VUV lamp for on-line gas analysis: setup and first results on cigarette smoke and human breath. Anal Chem 2005;77(22):7408–14.
[23] Shi L, Cheng X, Liu Q, Liu Z. Reaction of volatiles from a coal and various organic compounds during co-pyrolysis in a TG-MS system. Part 1. Reaction of volatiles in the void space between particles. Fuel 2018;213:37–47.
[24] Khan MR. A literature survey and an experimental study of coal devolatilization at mild and severe conditions: influences of heating rate, temperature, and reactor type on products yield and composition. Fuel 1989;68(12):1522–31.
[25] Okumura Y. Effect of heating rate and coal type on the yield of functional tar components. Proc Combust Inst 2017;36(2):2075–82.
[26] Lievens C, Ci D, Bai Y, Ma L, Zhang R, Chen JY, et al. A study of slow pyrolysis of one low rank coal via pyrolysis–GC/MS. Fuel Process Technol 2013;116:85–93.
[27] Yu G, Fan X, Liang P, Zhao G-M, Hu X. Online characterization of pyrolysis products and kinetics study for the pyrolysis of a coal. J Anal Appl Pyrol 2021;160:105376.
[28] Xu Y, Wang j, Zhang G, Zhang X, Zhang Y. The characteristics and mechanism for the formation of tars from low temperature pyrolysis of lignite. J Energy Inst 2021;99:248–55.
[29] Li X, Jin X, Wang M, Yu Y, Kong J, Xie W, et al. Effect of volatiles' reaction on coking of tar during pyrolysis of Naomaohu coal in a downer-bed reactor. Fuel Process Technol 2021;212:106623.
[30] Liu J, Zhong F, Niu W, Su J, Gao Z, Zhang K. Effects of heating rate and gas atmosphere on the pyrolysis and combustion characteristics of different crop residues and the kinetics analysis. At Energ 2019;175:320–32.
[31] Song G, Huang D, Li H, Wang X, Ren Q, Jiang L, et al. Pyrolysis reaction mechanism of typical Chinese agriculture and forest waste pellets at high heating rates based on the photo-thermal TGA. At Energ 2022;244:123164.
[32] Shi Z, Jin L, Zhou Y, Li Y, Hu H. Online analysis of initial volatile products of Shenhua coal and its macerals with pyrolysis vacuum ultraviolet photoionization mass spectrometry. Fuel Process Technol 2017;163:67–74.
[33] Wohlfahrt S, Fischer M, Saraji-Bozorgzad M, Matuschek G, Streibel T, Post E, et al. Rapid comprehensive characterization of crude oils by thermogravimetry coupled to fast modulated gas chromatography–single photon ionization time-of-flight mass spectrometry. Anal Bioanal Chem 2013;405(22):7107–16.

[34] Geißler R, Saraji-Bozorgzad M, Streibel T, Kaisersberger E, Denner T, Zimmermann R. Investigation of different crude oils applying thermal analysis/mass spectrometry with soft photoionisation. J Therm Anal Calorim 2009;96:813–20.
[35] Wen Y, Liu S, Fu S, Wang Z, Hu H, Jin L. Insight into influence of process parameters on co-pyrolysis interaction between Yulin coal and waste tire via rapid infrared heating. Fuel 2023;337:127161.
[36] Liu P, Le J, Wang L, Pan T, Lu X, Zhang D. Relevance of carbon structure to formation of tar and liquid alkane during coal pyrolysis. Appl Energy 2016;183:470–7.
[37] Gao M, Wang Y, Dong J, Li F, Xie K. Release behavior and formation mechanism of polycyclic aromatic hydrocarbons during coal pyrolysis. Chemosphere 2016;158(sep):1–8.
[38] Xiong Y, Jin L, Li Y, Zhou Y, Hu H. Structural features and pyrolysis behaviors of extracts from microwave-assisted extraction of a low-rank coal with different solvents. Energy Fuel 2019;33(1):106–14.
[39] Hu Q, Cheng W, Mao Q, Hu J, Yang H, Chen H. Study on the physicochemical structure and gasification reactivity of chars from pyrolysis of biomass pellets under different heating rates. Fuel 2022;314:122789.
[40] Efika CE, Onwudili JA, Williams PT. Influence of heating rates on the products of high-temperature pyrolysis of waste wood pellets and biomass model compounds. Waste Manage (Tucson, Ariz) 2018;76:497–506.
[41] Montoya J, Pecha B, Roman D, Janna FC, Garcia-Perez M. Effect of temperature and heating rate on product distribution from the pyrolysis of sugarcane bagasse in a hot plate reactor. J Anal Appl Pyrol 2017;123:347–63.
[42] Tian B, Qiao Yy, Tian Yy, Liu Q. Investigation on the effect of particle size and heating rate on pyrolysis characteristics of a bituminous coal by TG–FTIR. J Anal Appl Pyrol 2016;121:376–86.
[43] Yan L, Bai Y, Zhao R, Li F, Xie K. Correlation between coal structure and release of the two organic compounds during pyrolysis. Fuel 2015;145:12–7.
[44] Xiong Z, Wang Y, Syed-Hassan SSA, Hu X, Han H, Su S, et al. Effects of heating rate on the evolution of bio-oil during its pyrolysis. Energ Convers and Manag. 2018;163:420–7.